Moving Boundary Models for Dynamic Simulations of Two-Phase Flows

Munch Jensen, Jakob; Tummescheit, Hubertus

Published in:
Modelica'2002 Proceedings

2002

Jensen J.M., Tummescheit H.:

Moving Boundary Models for Dynamic Simulations of Two-Phase Flows

2nd International Modelica Conference, Proceedings, pp. 235-244

Paper presented at the 2nd International Modelica Conference, March 18-19, 2002,
Deutsches Zentrum für Luft- und Raumfahrt e.V. (DLR), Oberpfaffenhofen, Germany.

All papers of this workshop can be downloaded from
http://www.Modelica.org/Conference2002/papers.shtml

Moving Boundary Models for Dynamic Simulations of Two-Phase Flows

Jakob Munch Jensen[†] and Hubertus Tummescheit[‡]

[†]Department of Mechanical Engineering
Technical University of Denmark
jmj@mek.dtu.dk

[‡]Department of Automatic Control
Lund University, Sweden
hubertus@control.lth.se

Abstract

Two-phase flows are commonly found in components in energy systems such as evaporators and boilers. The performance of these components depends among others on the controller. Transient models describing the evaporation process are important tools for determining control parameters, and fast low order models are needed for this purpose. This article describes a general moving boundary (MB) model for modeling of two-phase flows.

The new model is numerically fast compared to discretized models and very robust to sudden changes in the boundary conditions. The model is a 7^{th} order model (7 state variables), which is a suitable order for control design. The model is also well suited for open loop simulations for systems design and optimization. It is shown that the average void fraction has a significant influence on the system response. A new method to calculate the average void fraction including the influence of the slip ratio is given. The average void fraction is calculated as a symbolic solution to the integral of the liquid fraction profile.

1 Introduction

First principle mathematical models of dynamical systems are made for a range of purposes, but one of the most common ones is to develop and verify controllers. The complexity of the model should be in accordance with the purpose of the model and this simple principle suggests that models for control design should be of low order and preferably easy to linearize. Unfortunately, physical systems are not sticking to this class of models, on the contrary: most mathematical first principle models are of distributed nature. The natural way to describe such a model is partial differential equations (PDE). PDE are infinite dimensional and their common numerical approximations, spatially discretized PDEs using one of the many possible discretization schemes, are of high order and without further model reduction not well suited for control design. The problem of control-oriented modeling is to derive a model which at the same time fulfills the requirements of control theory and characterizes those features of the system which are needed to satisfy the controller specification.

Moving boundary models for two phase flows in heat exchangers are a good example of low order control design models. They can be used for evaporators, condensers and steam generators. Their only disadvantage is that a number of mathematically rather different models arise depending on the operating conditions of the heat exchanger and the fluid conditions at the inlet of the equipment.

The model presented in this paper covers the most general case of two-phase heat exchangers with subcooled liquid at the inlet and superheated vapour at the outlet. This flow configuration is commonly found in thermal power systems, and the model can easily be extended to condensers and heat exchangers with subcooled liquid at the inlet and two-phase at the outlet. The special case of dry-expansion evaporators for refrigeration has been derived in [6].

The idea of a moving boundary model is to dynamically track the lengths of the different regions in the heat exchanger: the length from the inflow to the onset of boiling and the length of the two phase region. Simulation results are given for an evaporator in an organic rankine cycle, which utilizes the waste heat from a gas turbine in a small power plant. Other references to MB models include B.T. Beck that describes a MB-model for incomplete vaporization [2], a two region MB-model by He [4] and a three region model by Willatzen [7].

Roman and Greek Letters			
A	area	h	enthalpy
C_v	nozzle coef.	$\dot{m}$	mass flow
C_w	heat cap. of wall	q	heat flux
D	diameter	t	time
L	length	v	velocity
S	slip ratio	x	mass fraction
V_{cyl}	cylinder volume	z	length coordinate
α	heat transfer coef.	ρ	density
η	liquid fraction	ω	pump speed
η_v	volumetric efficiency	Φ	dissipation function
γ	void fraction	Ψ	vapour generation
μ	density ratio		
Subscripts			
1	subcooled	i	inner
2	two-phase	in	inlet
3	superheated	l	saturated liquid
12	interface 1-2	o	outer
23	interface 2-3	out	outlet
amb	ambient	r	refrigerant
c	condensation	w	wall
g	saturated gas		
Superscripts			
$'$	flux per length	$''$	flux per area
$'''$	flux per volume		

Table 1: Notation used in the Moving Boundary Model

2 Governing Equations

The general differential mass balance is

$$\frac{\partial \rho}{\partial t} + \nabla \cdot (\rho \vec{v}) = 0 \tag{1}$$

which for the one-dimensional case can be written as

$$\frac{\partial A\rho}{\partial t} + \frac{\partial \dot{m}}{\partial z} = 0 \tag{2}$$

The general differential energy balance is

$$\frac{\partial \rho h}{\partial t} + \nabla \cdot (\rho h \vec{v}) = -\nabla \cdot \vec{q}'' - q''' + \frac{Dp}{Dt} + \Phi \tag{3}$$

which can be simplified by neglecting the axial conductivity, radiation and the viscous stresses and assuming one dimensional flow:

$$\frac{\partial (A\rho h - Ap)}{\partial t} + \frac{\partial \dot{m} h}{\partial z} = \pi D \alpha (T_w - T_r). \tag{4}$$

A simplified differential energy balance for the wall is achieved by setting all flow terms in (3) equal to zero and neglecting the axial conductivity.

$$C_w \rho_w A_w \frac{\partial T_w}{\partial t} = \alpha_i \pi D_i (T_r - T_w) + \alpha_o \pi D_i (T_{amb} - T_w) \tag{5}$$

Equations (2), (4) and (5) are the differential balance equations, which will be integrated over the three regions to give the general three region lumped model for a two-phase heat exchanger. A schematic of the model is given in Figure 2. It is assumed in the following analysis that the change in pressure along the evaporator pipe is negligible.

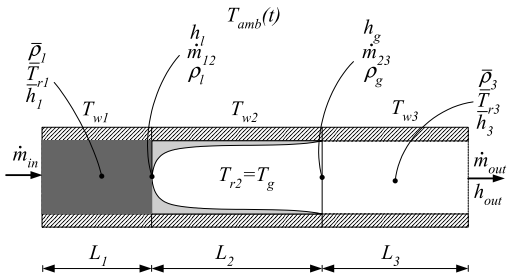

Figure 1: Schematic of the Three Region MB-model. 1 : subcooled, 2 : two-phase and 3 : superheated.

2.1 Mass Balance for the Subcooled Region

Integration of the mass balance (2) over the subcooled region gives

$$\int_0^{L_1} \frac{\partial (A\rho)}{\partial t} dz + \int_0^{L_1} \frac{\partial \dot{m}}{\partial z} dz = 0 \tag{6}$$

Applying Leibniz's rule (see Appendix A) on the first term and integrating the second term give for a constant area pipe:

$$A \frac{d}{dt} \int_0^{L_1} \rho dz - A\rho(L_1) \frac{dL_1}{dt} + \dot{m}_{12} - \dot{m}_{in} = 0. \tag{7}$$

The density at the interface $\rho(L_1)$ is equal to the saturated liquid density ρ_l. Pressure and mean enthalpy $\bar{h}_1$ define the state of the subcooled region where

$$\bar{h}_1 = \frac{1}{2}(h_{in} + h_l) \tag{8}$$

The inlet enthalpy h_{in} is known from the boundary conditions and h_l is a function of the pressure. The mean density in the subcooled region is approximated by

$$\bar{\rho}_1 = \frac{1}{L_1} \int_0^{L_1} \rho dz \approx \rho(p, \bar{h}_1) \tag{9}$$

The mean temperature is calculated from the same states as $\bar{T}_1 \approx T(p, \bar{h}_1)$. The mass balance for the subcooled region can be rewritten as

$$A \left\{ (\bar{\rho}_1 - \rho_l) \frac{dL_1}{dt} + L_1 \frac{d\bar{\rho}_1}{dt} \right\} = \dot{m}_{in} - \dot{m}_{12} \tag{10}$$

The term $d\bar{\rho}_1/dt$ is calculated using the chain rule:

$$\begin{aligned}\frac{d\bar{\rho}_1}{dt} &= \frac{\partial\bar{\rho}_1}{\partial p}\Big|_h \frac{dp}{dt} + \frac{\partial\bar{\rho}_1}{\partial\bar{h}_1}\Big|_p \frac{d\bar{h}_1}{dt} \\ &= \Big(\frac{\partial\bar{\rho}_1}{\partial p}\Big|_h + \frac{1}{2}\frac{\partial\bar{\rho}_1}{\partial\bar{h}_1}\Big|_p \frac{dh_l}{dp}\Big)\frac{dp}{dt} \\ &\quad + \frac{1}{2}\frac{\partial\bar{\rho}_1}{\partial\bar{h}_1}\Big|_p \frac{dh_{in}}{dt}\end{aligned} \tag{11}$$

The term dh_{in}/dt is determined from the boundary conditions to the heat exchanger model. The expression for $d\bar{\rho}_1/dt$ is inserted into the mass balance (10), such that the final mass balance for the subcooled region reads:

$$\begin{aligned}&A\Big\{(\bar{\rho}_1-\rho_l)\frac{dL_1}{dt} + L_1\Big(\frac{\partial\bar{\rho}_1}{\partial p}\Big|_h + \frac{1}{2}\frac{\partial\bar{\rho}_1}{\partial\bar{h}_1}\Big|_p \frac{dh_l}{dp}\Big)\frac{dp}{dt} \\ &+\frac{1}{2}L_1\frac{\partial\bar{\rho}_1}{\partial\bar{h}_1}\Big|_p \frac{dh_{in}}{dt}\Big\} = \dot{m}_{in} - \dot{m}_{12}.\end{aligned} \tag{12}$$

2.2 Energy Balance for the Subcooled Region

Integration of the energy balance (4) over the subcooled region gives

$$\begin{aligned}\int_0^{L_1}\frac{\partial(A\rho h - Ap)}{\partial t}dz + \int_0^{L_1}\frac{\partial\dot{m}h}{\partial z}dz \\ = \int_0^{L_1}\pi D\alpha(T_w - T_r)dz.\end{aligned} \tag{13}$$

Applying Leibniz's rule on the first term and integrating the other terms give for a constant area pipe and a constant heat transfer coefficient α

$$\begin{aligned}&A\frac{d}{dt}\int_0^{L_1}\rho h dz - A\rho(L_1)h(L_1)\frac{dL_1}{dt} - AL_1\frac{dp}{dt} \\ &+\dot{m}_{12}h_l - \dot{m}_{in}h_{in} = \pi D_i\alpha_{i1}L_1(T_{w1}-\bar{T}_{r1}).\end{aligned} \tag{14}$$

The first two terms are evaluated as

$$\begin{aligned}&\frac{d}{dt}\int_0^{L_1}\rho h dz - \rho(L_1)h(L_1)\frac{dL_1}{dt} \\ &= \frac{d}{dt}\big(\bar{\rho}_1\bar{h}_1L_1\big) - \rho_l h_l\frac{dL_1}{dt} \\ &= \Big(\frac{1}{2}\bar{\rho}_1(h_{in}+h_l) - \rho_l h_l\Big)\frac{dL_1}{dt} \\ &\quad + \frac{1}{2}L_1\Big(\bar{\rho}_1 + \frac{1}{2}(h_{in}+h_l)\frac{\partial\bar{\rho}_1}{\partial\bar{h}_1}\Big|_p\Big)\frac{dh_{in}}{dt} \\ &\quad + \frac{1}{2}L_1\Big\{\bar{\rho}_1\frac{dh_l}{dp} + (h_{in}+h_l) \\ &\quad \Big(\frac{\partial\bar{\rho}_1}{\partial p}\Big|_h + \frac{1}{2}\frac{\partial\bar{\rho}_1}{\partial\bar{h}_1}\Big|_p\frac{dh_l}{dp}\Big)\Big\}\frac{dp}{dt}.\end{aligned} \tag{15}$$

where $\bar{\rho}_1\bar{h}_1 \approx \overline{\rho_1 h_1} = \int_0^{L_1}\rho h dz$. The above equation (15) is inserted into the energy balance (14), which gives the final energy balance for the subcooled region:

$$\begin{aligned}&\frac{1}{2}A\Big\{\Big(\bar{\rho}_1(h_{in}+h_l) - 2\rho_l h_l\Big)\frac{dL_1}{dt} \\ &\quad + \Big(\bar{\rho}_1 L_1 + \frac{\partial\bar{\rho}_1}{\partial h}\Big|_p\Big)\frac{dh_{in}}{dt} \\ &\quad + L_1\Big\{\bar{\rho}_1\frac{dh_l}{dp} + (h_{in}+h_l)\cdot \\ &\quad \Big(\frac{\partial\bar{\rho}_1}{\partial p}\Big|_h + \frac{1}{2}\frac{\partial\bar{\rho}_1}{\partial h}\Big|_p\frac{dh_l}{dp} - 2\Big)\Big\}\frac{dp}{dt}\Big\} \\ &= \dot{m}_{in}h_{in} - \dot{m}_{12}h_l + \pi D_i L_1\alpha_{i1}(T_{w1} - \bar{T}_{r1}).\end{aligned} \tag{16}$$

2.3 Mass and Energy Balances for the Two-Phase and Superheated Regions

The mass and energy balances are integrated over the two-phase region and the superheated region using the same procedure as for the subcooled region. The equations are derived in detail in Appendix B.

The flow in the two-phase region is assumed to be homogeneous at equilibrium conditions with a mean density of $\bar{\rho} = \bar{\gamma}\rho_g + (1-\bar{\gamma})\rho_l$, where the void fraction is defined as $\gamma = A_g/A$. The average void fraction is defined as $\bar{\gamma} = \frac{1}{L_2}\int_{L_1}^{L_1+L_2}\gamma dz$ and is assumed to be invariant with time. A detailed model of the calculation of the void fraction is derived in section 2.5. The mass balance for the two-phase region is

$$\begin{aligned}&A\Big\{(\rho_l-\rho_g)\frac{L_1}{dt} + (1-\bar{\gamma})(\rho_l-\rho_g)\frac{dL_2}{dt} \\ &\quad + L_2\Big(\bar{\gamma}\frac{d\rho_g}{dp} + (1-\bar{\gamma})\frac{d\rho_l}{dp}\Big)\frac{dp}{dt}\Big\} = \dot{m}_{12} - \dot{m}_{23}\end{aligned} \tag{17}$$

and the energy balance for the two-phase region is

$$\begin{aligned}&A\Big\{L_2\Big\{\bar{\gamma}\frac{d(\rho_g h_g)}{dp} + (1-\bar{\gamma})\frac{d(\rho_l h_l)}{dp} - 1\Big\}\frac{dp}{dt} \\ &+\Big\{\bar{\gamma}\rho_g h_g + (1-\bar{\gamma})\rho_l h_l\Big\}\frac{dL_1}{dt} \\ &+\Big\{(1-\bar{\gamma})\big(\rho_l h_l - \rho_g h_g\big)\frac{dL_2}{dt} \\ &= \dot{m}_{12}h_l - \dot{m}_{23}h_g + \pi D_i\alpha_{i2}L_2(T_{w2}-T_{r2})\end{aligned} \tag{18}$$

The derivative of the properties at the phase boundaries are written in a short notation and can be rewritten as e.g. $d(\rho_g h_g)/dp = h_g(d\rho_g/dp) + \rho_g(d\rho_g/dp)$. Both $d(\rho_g h_g)/dp$ and $d(\rho_l h_l)/dp$ can be calculated

from the pressure. The mass balance for the superheated region reads:

$$\begin{aligned} A\Big\{ & L_3\Big(\frac{1}{2}\frac{\partial\bar{\rho}_3}{\partial\bar{h}_3}\Big|_p\frac{dh_g}{dp}+\frac{\partial\bar{\rho}_3}{\partial p}\Big|_h\Big)\frac{dp}{dt} \\ & (\rho_g-\bar{\rho}_3)\frac{dL_1}{dt}+(\rho_g-\bar{\rho}_3)\frac{dL_2}{dt} \\ & +\frac{1}{2}L_3\frac{\partial\bar{\rho}_3}{\partial\bar{h}_3}\Big|_p\frac{dh_{out}}{dt}\Big\}=\dot{m}_{23}-\dot{m}_{out}. \end{aligned} \tag{19}$$

The energy balance for the superheated region is given by

$$\begin{aligned} A\Big\{ & \Big(\rho_g h_g-\frac{1}{2}\bar{\rho}_3(h_g+h_{out})\Big)\Big(\frac{dL_1}{dt}+\frac{dL_2}{dt}\Big) \\ & +L_3\Big[\frac{1}{2}(h_g+h_{out})\Big(\frac{1}{2}\frac{\partial\bar{\rho}_3}{\partial\bar{h}_3}\Big|_p\frac{dh_g}{dp}+\frac{\partial\bar{\rho}_3}{\partial p}\Big|_h\Big) \\ & +\frac{1}{2}\bar{\rho}_3\frac{dh_g}{dp}-1\Big]\frac{dp}{dt} \\ & \Big(\frac{1}{2}\bar{\rho}_3L_3+\frac{1}{4}\frac{\partial\bar{\rho}_3}{\partial\bar{h}_3}\Big|_p(h_g+h_{out})L_3\Big)\frac{dh_{out}}{dt} \\ & =\dot{m}_{23}h_g-\dot{m}_{out}h_{out}+\pi D_i\alpha_{i3}L_3(T_{w3}-\bar{T}_{r3}) \end{aligned} \tag{20}$$

The mean properties of the superheated region are calculated in the same way as in the subcooled region. Thus $\bar{h}_3=0.5(h_g+h_{out})$, $\bar{\rho}_3\approx\rho(p,\bar{h}_3)$ and $\bar{T}_{r3}\approx T(p,\bar{h}_3)$.

2.4 Energy Balance for the Wall Regions

The energy balances for the walls are derived. Integration of the wall energy equation (5) from α to β gives

$$\begin{aligned} \int_\alpha^\beta C_w\rho_w A_w\frac{\partial T_w}{\partial t}dz= & \int_\alpha^\beta\alpha_i\pi D_i(T_r-T_w)dz \\ & +\int_\alpha^\beta\alpha_o\pi D_i(T_{amb}-T_w)dz \end{aligned} \tag{21}$$

Applying Leibniz's rule, assuming constant wall properties give and rearranging gives the general energy balance for a wall region:

$$\begin{aligned} C_w\rho_w A_w\Big\{ & (\beta-\alpha)\frac{dT_w}{dt}+\big(T_w(\alpha)-T_w\big)\frac{d\alpha}{dt} \\ & +\big(T_w-T_w(\beta)\big)\frac{d\beta}{dt}\Big\}=\alpha_i\pi D_i(\beta-\alpha)\big(T_r-T_w\big) \\ & +\alpha_o\pi D_o(\beta-\alpha)\big(T_{amb}-T_w\big). \end{aligned} \tag{22}$$

For the wall region adjacent to the subcooled region $\alpha=0$ and $\beta=L_1$, which gives

$$\begin{aligned} & C_w\rho_w A_w\Big\{L_1\frac{dT_{w1}}{dt}+\big(T_{w1}-T_w(L_1)\big)\frac{dL_1}{dt}\Big\} \\ & =\alpha_i 1\pi D_i L_1\big(T_{r1}-T_{w1}\big)+\alpha_o\pi D_o L_1\big(T_{amb}-T_{w1}\big) \end{aligned} \tag{23}$$

The wall temperature in the model is discontinuous at L_1 giving

$$\begin{aligned} T_w(L_1)&=T_{w2}\text{ for }\frac{dL_1}{dt}>0 \\ T_w(L_1)&=T_{w1}\text{ for }\frac{dL_1}{dt}\le 0 \end{aligned} \tag{24}$$

Similar expressions are derived for the walls adjacent to the two-phase and the superheated regions see Appendix B. Typically in the literature a simplified mean value for $T_w(L_1)$ has been used, which seems attractive in order to simplify the model see e.g. [4] and [7]. Simulations show that the response times for the system for some test conditions depend significantly on the expression for $T_w(L_1)$, and the full equations given by (23) and (24) should therefore be used.

The general three region moving boundary model is described by the mass and energy balances for the flow stated in equations (12), (16), (17), (18), (19) and (20) and the energy balances for the wall regions as stated in equations (23), (49) and (51). In addition the two discontinuous equations for the wall temperatures as stated in (24) and (50) are needed. This equation system contains 9 equations with the 7 state variables: $(L_1,L_2,p,h_{out},T_{w1},T_{w2}$ and $T_{w3})$. The variable h_{in}, which also appears differentiated, is calculated as a boundary condition and is thus not included in the state variables for the MB-model. Dependent variables can be calculated from the state variables and include: $(\bar{\rho}_1,\rho_l,\rho_g,\bar{\rho}_3,\partial\bar{\rho}_1/\partial\bar{h}_1|_p,\partial\bar{\rho}_1/\partial p|_h,d\rho_l/dp,d\rho_g/dp,$ $\partial\bar{\rho}_3/\partial\bar{h}_1|_p,\partial\bar{\rho}_3/\partial p|_h,\bar{h}_1,h_l h_g,\bar{h}_3,dh_l/dp,dh_g/dp,\bar{T}_{r1},$ $\bar{T}_{r2},\bar{T}_{r3},\dot{m}_{12},\dot{m}_{23})$. Parameters are constant during simulation and include: $(A,D_i,D_o,\alpha_{i1},\alpha_{i2},\alpha_{i3},\alpha_o,\bar{\gamma},L,T_{amb},C_w,\rho_w,A_w)$. The boundary models calculate the variables $(\dot{m}_{in},\dot{m}_{out},h_{in}$ and $dh_{in}/dt)$, which are boundary conditions to the MB-model.

2.5 Calculation of the Average Liquid Fraction $\bar{\eta}$

The liquid fraction in the two phase region $\eta(z)$ is related to the void fraction $\gamma(z)$ via the equation

$$\eta(z)+\gamma(z)=1. \tag{25}$$

The same equation holds for the average values $\bar{\eta}$ and $\bar{\gamma}$ over the whole region, which are the parameters of interest. It is computed as the integral over the normalized profile. For the derivation of a $\eta(z)$ profile, a couple of assumptions are necessary:

1. All assumptions made in the derivation of the moving boundary model apply also to the derivation of the liquid fraction profile, in particular that a constant pressure is assumed along the pipe.

2. The profile can be evaluated under steady state conditions. For the purpose of slow, start-up transients as well as for linearization purposes this does not pose any restrictions. This means in particular that the pressure is in steady state.

3. The vapour generation rate Ψ' is uniform over the evaporator length.

4. The slip velocity ratio $S = u_g/u_l$ between the gas and the liquid velocities is constant along the evaporator length and a known function of the model states that also can be evaluated under steady state conditions[1].

A similar derivation but assuming a slip velocity ratio of 1 has been done in [3]. Under the above assumptions, the following coupled ODE boundary value problem holds:

$$\rho_l \frac{\partial(A_l u_l)}{\partial z} = -\Psi' \quad (26)$$

$$\rho_g \frac{\partial(A_g u_g)}{\partial z} = \Psi' \quad (27)$$

Ψ' is the net generation of saturated vapour per unit length $[kg/(ms)]$, A_l and A_g are the cross sectional areas taken up by liquid and vapour respectively and the densities are independent of the length coordinate because we assumed no pressure loss and steady state conditions for the pressure. This equation is normalized by setting $A = A_l + A_g = 1$ and letting the length of the evaporation region run from 0 to 1 so that the cross section area $A_l(z)$ is now equivalent to the liquid volume fraction $\eta(z)$. Then, replacing u_l with u and u_g with Su and dividing by ρ_l the following normalized equation is obtained:

$$\frac{\partial(\eta u)}{\partial z} = -\Psi^* \quad (28)$$

$$\mu S \frac{\partial((1-\eta)u)}{\partial z} = \Psi^* \quad (29)$$

[1]Remark: It is possible to weaken this assumption and use a slip ratio $S(z)$ which is a function of the length coordinate. Many of the rather complex empirical slip correlations depend on the local mass fraction $x = \dot{m}_g/\dot{m}$ as well and in this case the profile and the integral over the profile can only be solved numerically. For certain applications this may result in the most accurate approximation of the mean void fraction.

where

$$\Psi^* = \frac{\Psi}{\rho_l A}, \quad \text{and} \quad \mu = \frac{\rho_g}{\rho_l}.$$

The boundary conditions at the length coordinates $z = 0.0$ and $z = 1.0$ are

$$\eta(0) = 1, \qquad \eta(1) = 0. \quad (30)$$

From (28), (29) and the boundary conditions, the following function for $\eta(z)$ can be derived:

$$\eta(z) = \frac{1-z}{1+z\left(\frac{1}{S\mu}-1\right)} \quad (31)$$

The influence of the slip ratio S on the amount of saturated liquid in the evaporation region, $\bar{\eta}$ can seen in Figure 2. $\eta(z)$ can be integrated symbolically to give:

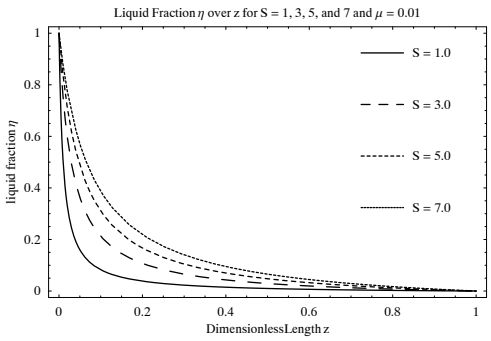

Figure 2: Liquid Fraction $\eta(z)$ along the normalized evaporation region.

$$\bar{\eta} = \int_0^1 \eta(z)dz = \frac{S\mu\,(S\mu - 1 - ln(S\mu))}{(S\mu-1)^2} \quad (32)$$

This $\bar{\eta}$ can only be used together with the dynamic model from the previous section when the time derivative of $\bar{\eta}$ can be neglected. This holds for slow pressure transients. The density ratio μ is a unique and simple function of the pressure, but for the slip ratio S a number of empirical correlations are available to choose from. Because of the assumptions made above, we have to choose a slip ratio which is independent of the local void fraction or mass fraction. A simple and appealing correlation is the one from Zivi (1964) cited in [9] which minimizes the total kinetic energy flow locally at each position z along the pipe:

$$S = \frac{u_g}{u_l} = \left(\frac{\rho_l}{\rho_g}\right)^{1/3} = \mu^{1/3} \quad (33)$$

Using this slip correlation, the average liquid fraction in the pipe becomes a function of only one variable,

the density ratio μ.

$$\bar{\eta} = \int_0^1 \eta(z)dz = \frac{1+(1/\mu)^{2/3}(2/3\,ln\,(1/\mu)-1)}{\left((1/\mu)^{2/3}-1\right)^2} \tag{34}$$

Both the density ratio μ and the slip S approach 1 when the pressure is rising toward the critical pressure. In the limit, the liquid and vapour densities are equal as well as the flow speeds, so that a mean liquid fraction of 0.5 is expected, compare the plot of $\bar{\eta}$ in Figure 3.

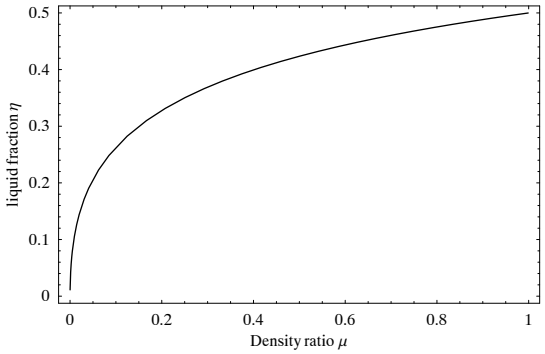

Figure 3: Average Liquid fraction $\bar{\eta}$ as a function of the density ratio μ.

3 Dominating Time Constants of the Linearized Model

In this section the influence of some model parameters on the eigenvalues of a linearization of the system derived in section 2 is investigated. Models for fluid flow exhibit two types of time constants: fast, hydraulic time constants for disturbances traveling with the speed of sound and much slower thermal ones, whose disturbances move at the flow speed. In two phase flows, the coupling between thermal and hydraulic phenomena is much tighter than in one phase flows, because a change in the hydraulic pressure is tightly coupled to a change in the temperature. The eigenvectors reveal that the 7 eigenvalues are tightly coupled, but roughly their physical interpretation is as follows:

- one mode comes from the overall mass balance of the evaporator which depends on the ratio between the total mass and the sum of the mass flows in and out of the evaporator and
- one for the overall energy balance which depends on the ratio of the total heat capacity to the sum of convective and heat transfer energy flows,
- one for each of the lengths of the subcooled and the two-phase regions. These are a combination of the mass and energy balances for the respecitive region.
- Three more eigenvalues come from the energy balances of the evaporator walls.

In [1] Bauer derived a more detailed, distributed model of heterogeneous flow[2] and validated it against measurement data for the refrigerant R22. According to [1], the advantage of the heterogenous model over the homogeneous one is that the void fraction turns out to be more realistic. Therefore, the dominant time constants are modeled more accurately. The average void fraction $1-\bar{\eta}$ has a strong influence on the total fluid mass in the evaporator, as can be seen clearly from Figure 4. It can be concluded from this argument that

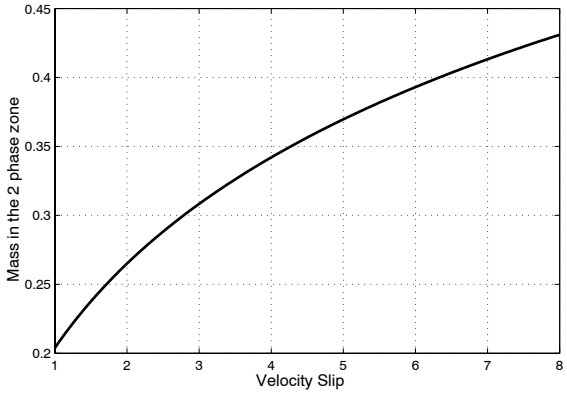

Figure 4: Total mass in the two-phase region as a function of velocity slip.

the void fraction $\bar{\gamma}$ is a crucial parameter in the moving boundary model. Using a good approximation of the void fraction, which may be obtained from a detailed, distributed model like in [1], is important for obtaining realistic dynamic behaviour.

The slow modes in the overall system are mostly influenced by the wall temperatures: higher heat capacities and smaller heat transfer coefficients result in slower modes. This means that the slowest mode usually is governed by the pipe wall in the liquid region. Two model parameters with a large influence on the slow time constants are the void fraction $\bar{\gamma}$ and the ratio of the total heat capacities of fluid and pipe walls of the evaporator pipes. The latter depend on the system pressure and the pipe diameter. Correct estimation of

[2]Heterogeneous flow means that the flow speeds of the gas and liquid phases can be different. A homogeneous flow assumption is equivalent to the same flow speed for both phases.

the void fraction gets more important at lower pressures because the slip increases due to smaller density ratio μ and the heat capacity of the pipes is usually smaller due to thinner pipe walls.
The root locus plot in Figure 5 shows the slow eigenvalues of the system, which are the dominating ones for control design purposes. These vary significantly when the slip ratio S (and thus the void fraction) is varied from 1.0 to 8.0. In the example with approx. 31 bars the pressure is relatively high for the working fluid R22 and therefore the slip ratio is not very far from 1. Nonetheless, the slow eigenvalues move considerably on the root locus. The change in the model dynamics will be larger at lower pressures.

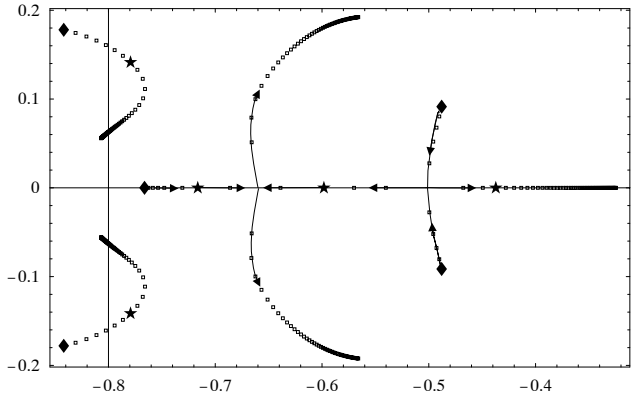

Figure 5: Root Locus for the slow eigenvalues. Diamonds mark a slip ratio of 1.0, stars a slip ratio of the test case of ≈ 1.7. Slip ratios vary from 1.0 to 8.0.

4 Model Variants

The main effect of using a velocity slip estimate to calculate the average void fraction is an improved model of the fluid mass in the evaporator. In a model for control design around a narrow operating pressure – the short transient case – a constant void fraction based on the profile derived above, will give sufficiently accurate results. Different slip correlations than the one from above and numerical quadrature can be used to find a good estimate of the mean void fraction. A fixed void fraction will be less adequate when "long" transients over wide pressure ranges are to be simulated. During the simulation of the start-up of a near- or supercritial once-through boiler, which is a classical case for a moving boundary model (see [3]), the density ratio μ will change by 3 orders of magnitude. In that case the simple slip correlation $S = \mu^{1/3}$ works well to model the fluid mass in the evaporator.

The model derived above is still too complex and has too many states for some purposes, e. g., online dynamic optimization as it is done in Model Predictive Control (MPC). There are several ways to reduce the number of states in the moving boundary model. One possibility is to assume that the 2-phase heat transfer coefficient is much higher than the outer heat transfer coefficient so that the wall temperature and the fluid temperature in the evaporation region are equal. This assumption may also be extended to the subcooled and superheated regions. The model will loose accuracy in the high frequency range but will be very similar to the full model at low frequency range. Another possible simplification is to get rid of the states in the superheated region, because it is usually short and contains only few percent of the fluid mass. The dynamic model for the region can be replaced by a semi-empirical algebraic relation for the superheat temperature, see [4]. Investigation of these options for model reduction is the goal of future work by the authors.

4.1 Boundary Models

The test simulations for the heat exchanger are performed for a simple cycle containing a pump that supplies the liquid flow into the evaporator and a nozzle (turbine) at the end of the evaporator. The pump model is defined by a simple expression for the mass flow

$$\dot{m}_{pump} = \eta_v \rho_{pump} V_{cyl} \omega \tag{35}$$

where η_v is the volumetric efficiency, ρ_{pump} is the inlet density to the pump, V_{cyl} is the cylinder volume and ω is the number of revolutions per second. The specific enthalpy at the inflow of the evaporator is h_{in} and is a constant below the saturated liquid enthalpy.
The model of the nozzle is computed as:

$$\dot{m}_{nozzle} = C_v \sqrt{\rho_{out}(p - p_c)}. \tag{36}$$

where C_v is a coefficient, ρ_{out} is the outlet density from the evaporator, p is the pressure in the evaporator and p_c is a constant pressure lower than p.

5 Simulation Result

The evaporator in an organic rankine cycle (ORC) is simulated using the three region moving boundary model and the models for the pump and the nozzle. The simulation program Dymola [5] has been used to perform the simulations. The ORC is used to convert thermal energy to electric energy in applications

with small temperature differences between the high and the low temperature heat sources. The ORC can thereby be used to improve the energy efficiency in gas turbine power plants by converting the waste heat energy in the exhaust gas to electricity. Simulation results for a test case of an evaporator pipe are shown in Figure 6 to Figure 8.

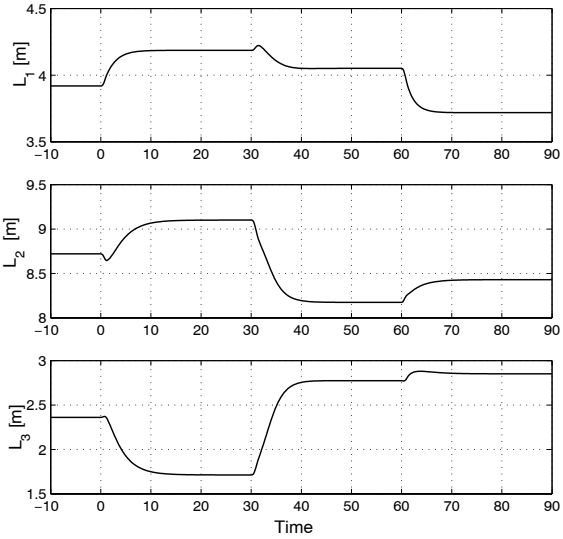

Figure 6: Lengths of the three regions

Pump and nozzle parameters	
$\eta_v = 0.6$ [-]	$C_v = 3.76E-5$ $[m^2]$
$\omega = 60$ $[rps]$	$p_c = 1.4$ $[Mpa]$
$V_{cyl} = 1.30E-5$ $[m^3]$	
Evaporator steady state results	
$L = 15$ $[m]$	$Q = 163$ $[kW]$
$D_i = 0.020$ $[m]$	$\dot{m} = 0.54$ $[kg/s]$
$D_o = 0.022$ $[m]$	$p = 3.6$ $[Mpa]$
$C_w = 385$ $[J/kgK]$	$T_{w1} = 388.8$ $[K]$
$\rho_w = 8.96E3$ $[kg/m^3]$	$T_{w2} = 371.7$ $[K]$
$\alpha_{i1} = 2451$ $[J/m^2K]$	$T_{w3} = 449.5$ $[K]$
$\alpha_{i2} = 11404$ $[J/m^2K]$	$T_{r1} = 306.0$ $[K]$
$\alpha_{i3} = 2071$ $[J/m^2K]$	$T_{r2} = 352.3$ $[K]$
$\alpha_o = 500$ $[J/m^2K]$	$T_{r3} = 384.0$ $[K]$
$T_{amb} = 573.1$ $[K]$	$L_1 = 3.9$[m]
$S = 1.67$ [-]	$L_2 = 8.7$[m]
$\bar{\gamma} = 0.665$ [-]	$L_3 = 2.4$[m]

Table 2: Parameters and steady-state results

Three experiments are performed with parameters and initial steady state results in table 2. At $t = 0\ s$ the pump speed ω is increased by 5%, at $t = 30\ s$ the outer heat transfer coefficient α_o is increased by 10% and at $t = 60\ s$ the nozzle coefficient C_v is increased by 10%. Figure 6, 7 and 8 show the transient response of the system.

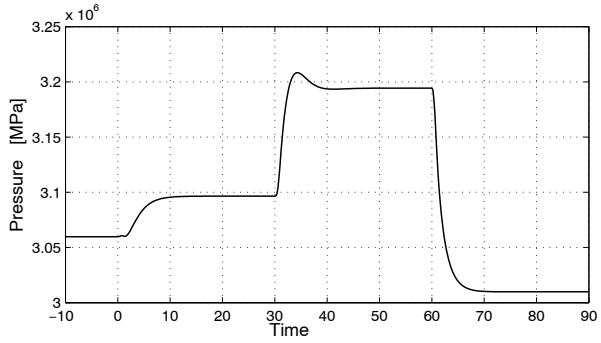

Figure 7: Pressure in the evaporator

The length of the subcooled and the two-phase region is seen to increase as the pump speed is increased (at t=0s). Also the pressure and the heating effect is increased which is expected. An increase in outer heat transfer (at t=30s) results in shorter two-phase and superheated regions as well as in increased heating effect. The larger nozzle coefficient ($t = 60\ s$) results in a decrease in pressure. The reduced pressure lowers the boiling point and thus the fluid temperature in the evaporation region. The length of the subcooled region is therefore shrinking. The length of the two-phase region grows in this case but this trend depends on the conditions. The lower evaporating temperature tends to decrease the length of the two-phase region and the larger latent heat increases it. The heating effect rises in this case, but this trend depends on the conditions as well. The model gives the right trends even though no experimental data has been available to validate the model.

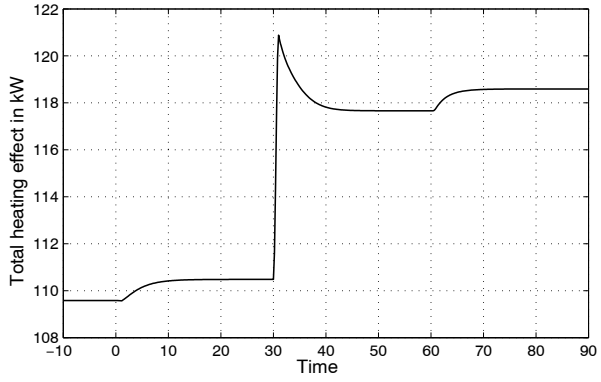

Figure 8: Heating effect to the evaporator

5.1 Conclusions

A new moving boundary model has been presented describing the dynamics of two phase heat exchang-

ers with liquid at the inlet and vapour at the outlet. The new model is numerically fast compared to discretized models and very robust to sudden changes in the boundary conditions. The model is a 7th order model (7 state variables), which is a suitable order for control design. The model is also well suited for open loop simulations for systems design and optimization. It is shown that the average void fraction has a significant influence on the system response. A new method to calculate the average void fraction including the influence of the slip ratio is presented. The average void fraction is computed from the symbolic solution to the integral of the liquid fraction profile.

Appendix A: Leibniz's Rule

Leibniz's rule for differentiation of integrals with time varying limits reads ([8]):

$$\frac{d}{dt}\int_{z_1}^{z_2} f(z,t)dz = f(z_2,t)\frac{dz_2}{dt} - f(z_1,t)\frac{dz_1}{dt} + \int_{z_1}^{z_2}\frac{\partial f(z,t)}{\partial t}dz. \tag{37}$$

Appendix B: Derivation of the Model Equations

Mass Balance for the Two-Phase Region

The mass balance (2) is integrated over the two-phase region from L_1 to L_1+L_2 Applying Leibniz's rule gives for a constant area pipe

$$\begin{aligned} A\frac{d}{dt}\int_{L_1}^{L_1+L_2}\rho dz + A\rho(L_1)\frac{dL_1}{dt} \\ - A\rho(L_1+L_2)\frac{d(L_1+L_2)}{dt} \\ + \dot{m}_{23} - \dot{m}_{12} = 0 \end{aligned} \tag{38}$$

The flow is assumed to be homogeneous at equilibrium conditions with a mean density of $\rho = \bar{\gamma}\rho_g + (1-\bar{\gamma})\rho_l$. The mass balance for the two-phase region becomes

$$\begin{aligned} A\left\{\frac{d}{dt}(\rho_2 L_2) + (\rho_l - \rho_g)\frac{dL_1}{dt} - \rho_g\frac{dL_2}{dt}\right\} \\ = \dot{m}_{12} - \dot{m}_{23} \end{aligned} \tag{39}$$

where $\rho_2 = \bar{\gamma}\rho_g + (1-\bar{\gamma})\rho_l$. The time derivative of ρ_2 is

$$\frac{d\rho_2}{dt} = \left(\bar{\gamma}\frac{d\rho_g}{dp} + (1-\bar{\gamma})\frac{d\rho_l}{dp}\right)\frac{dp}{dt} \tag{40}$$

which inserted into the mass balance (39) gives the final mass balance for the two-phase region as stated in (17).

Energy Balance for the Two-Phase Region

The energy balance (4) is integrated over the two-phase region from L_1 to L_1+L_2. Applying Leibniz's rule gives for a constant area pipe

$$\begin{aligned} A\frac{d}{dt}\int_{L_1}^{L_1+L_2}\rho h dz + A\rho(L_1)h(L_1)\frac{dL_1}{dt} - AL_1\frac{dp}{dt} \\ - A\rho(L_1+L_2)h(L_1+L_2)\frac{d(L_1+L_2)}{dt} - AL_2\frac{dp}{dt} \\ + \dot{m}_{23}h_g - \dot{m}_{12}h_l = \pi D_i\alpha_{i2}L_2(T_{w2} - T_{r2}) \end{aligned} \tag{41}$$

The first term is evaluated as

$$\begin{aligned} \frac{d}{dt}\int_{L_1}^{L_1+L_2}\rho h dz &= \frac{d}{dt}\int_{L_1}^{L_1+L_2}\left(\gamma\rho_g h_g + (1-\gamma)\rho_l h_l\right)dz \\ &= \frac{d}{dt}\left\{\left(\bar{\gamma}\rho_g h_g + (1-\bar{\gamma})\rho_l h_l\right)L_2\right\} \\ &= L_2\left\{\bar{\gamma}\frac{d(\rho_g h_g)}{dp} + (1-\bar{\gamma})\frac{d(\rho_l h_l)}{dp}\right\}\frac{dp}{dt} \\ &\quad + \left\{\bar{\gamma}\rho_g h_g + (1-\bar{\gamma})\rho_l h_l\right\}\frac{dL_2}{dt} \end{aligned} \tag{42}$$

Inserting (42) into (41) gives the final energy balance for the two-phase region as state in (18).

Mass Balance for the Superheated Region

The mass balance (2) is integrated over the superheated region from L_1+L_2 to L which for a constant area pipe gives

$$\int_{L_1+L_2}^{L}\frac{\partial A\rho}{\partial t}dz + \int_{L_1+L_2}^{L}\frac{\partial \dot{m}}{\partial z}dz = 0 \tag{43}$$

Applying Leibniz's rule on the first term and integrating the second term give for a constant area pipe

$$\begin{aligned} A\frac{d}{dt}\int_{L_1+L_2}^{L}\rho dz + A\rho(L_1+L_2)\frac{d(L_1+L_2)}{dt} \\ + \dot{m}_{out} - \dot{m}_{23} = 0 \end{aligned} \tag{44}$$

The mean density in the superheated region is $\rho_3 = \frac{1}{L_3}\int_{L_1+L_2}^{L}\rho dz \approx \rho(p,h_3)$, which inserted in the mass balance (44) gives

$$\begin{aligned} A\left\{L_3\frac{d\rho_3}{dt} + (\rho_g - \rho_3)\frac{dL_1}{dt} + (\rho_g - \rho_3)\frac{dL_2}{dt}\right\} \\ = \dot{m}_{23} - \dot{m}_{out} \end{aligned} \tag{45}$$

The derivative of ρ_3 is calculated as

$$\begin{aligned} \frac{d\rho_3}{dt} &= \frac{\partial\rho_3}{\partial p}\Big|_h\frac{dp}{dt} + \frac{\partial\rho_3}{\partial h}\Big|_p\frac{dh}{dt} \\ &= \left(\frac{1}{2}\frac{\partial\rho_3}{\partial h_3}\Big|_p\frac{dh_g}{dp} + \frac{\partial\rho_3}{\partial p}\Big|_h\right)\frac{dp}{dt} + \frac{1}{2}\frac{\partial\rho_3}{\partial h_3}\Big|_p\frac{dh_{out}}{dt} \end{aligned} \tag{46}$$

The expression for $\frac{d\rho_3}{dt}$ is inserted into (45), which gives the final mass balance for the superheated region as stated in (19).

Energy Balance for the Superheated Region

The energy equation 4 is integrated over the superheated region from L_1+L_2 to L. Applying Leibniz's rule gives for a constant area pipe

$$\begin{aligned} A\frac{d}{dt}\int_{L_1+L_2}^{L}\rho h dz + A\rho(L_1+L_2)h(L_1+L_2)\frac{d(L_2)}{dt} \\ - AL_3\frac{dp}{dt} + \dot{m}_{out}h_out - \dot{m}_{23}h_g \\ = \pi D_i\alpha_{i3}L_3(T_{w3}-T_{r3}) \end{aligned} \tag{47}$$

The first term is calculated as

$$\begin{aligned} \frac{d}{dt}\int_{L_1+L_2}^{L}\rho h dz &= \frac{d}{dt}(\bar{\rho}_3\bar{h}_3L_3) \\ &= -\frac{1}{2}\bar{\rho}_3(h_g+h_{out})\left(\frac{d(L_1+L_2)}{dt}\right) \\ &\quad + \frac{1}{2}L_3(h_g+h_{out})\frac{d\bar{\rho}_3}{dt} \\ &\quad + \frac{1}{2}\bar{\rho}_3L_3\left(\frac{dh_g}{dp}\frac{dp}{dt}+\frac{dh_{out}}{dt}\right) \end{aligned} \tag{48}$$

where $\bar{h}_3 = \frac{1}{2}(h_g+h_{out})$ and $\bar{\rho}_3 = \rho(p,\bar{h}_3)$. Equation (48) and the expression for $\frac{d\bar{\rho}_3}{dt}$ from equation (46) is inserted into (47), which after some rearranging gives the final energy balance for the superheated region as stated in (20).

Energy Balance for the Walls

For the wall region adjacent to the two-phase region $\alpha = L_1$ and $\beta = L_1+L_2$, which inserted in (22) gives

$$\begin{aligned} C_w\rho_wA_w\Big\{L_2\frac{dT_{w2}}{dt} + \big(T_w(L_1)-T_{w2}\big)\frac{dL_1}{dt} \\ + \big(T_{w2}-T_w(L_1+L_2)\big)\frac{dL_2}{dt}\Big\} \\ = \alpha_i 2\pi D_iL_2\big(T_{r2}-T_{w2}\big) \\ + \alpha_o\pi D_oL_2\big(T_{amb}-T_{w2}\big) \end{aligned} \tag{49}$$

$T_w(L_1)$ is given by (24), and $T_w(L_1+L_2)$ is given by

$$\begin{aligned} T_w(L_1+L_2) &= T_{w3} \text{ for } \frac{dL_2}{dt} > 0 \\ T_w(L_1+L_2) &= T_{w2} \text{ for } \frac{dL_2}{dt} \le 0 \end{aligned} \tag{50}$$

For the wall region adjacent to the superheated region $\alpha = L_1+L_2$ and $\beta = L$, which inserted in (22) gives

$$\begin{aligned} C_w\rho_wA_w\Big\{L_3\frac{dT_{w3}}{dt} + \big(T_w(L_1)-T_{w2}\big)\frac{dL_1}{dt} \\ + \big(T_w(L_1+L_2)-T_{w3}\big)\Big(\frac{dL_1}{dt}+\frac{dL_2}{dt}\Big)\Big\} \\ = \alpha_i 3\pi D_iL_3\big(T_{r3}-T_{w3}\big) + \alpha_o\pi D_oL_3\big(T_{amb}-T_{w3}\big) \end{aligned} \tag{51}$$

References

[1] Olaf Bauer, *Modelling of Two-Phase Flows with Modelica*, Masters Thesis ISRN LUTFD2/TRFT–5629–SE, Department of Automatic Control, Lund University, November 1999.

[2] B.T. Beck and G.L.Wedekind, *A generalization of the system mean void fraction model for transient two-phase evaporation flows*, Int. J. of Heat Transfer **103** (1981), 81 – 85.

[3] S. Bittanti, M. Bottinelli, A. De Marco, M. Facchetti, and W. Prandoni, *Performance Assessment of the Control System of Once-Through Boilers*, Proceedings of the 13th Conference on Process Control '01, June 2001.

[4] X.D. He and S. Liu, *Multivariable Control of Vapor Compression Systems*, HVAC Research **4** (1998), 205 – 230.

[5] http://www.dynasim.se.

[6] J.M̃. Jensen and H.J. Hoegaard Knudsen, *A new moving boundary model for transient simulations of dry-expansion evaporators*, Proceedings of the 15th International Conference on Efficiency, Costs, Optimization, Simulation and Environmental Impact of Energy Systems, July 2002.

[7] N.B.O.L. Pettit M. Willatzen and L. Plough-Sørensen, *A general dynamic simulation model for evaporators and condensers in refrigeration*, Int. J. of Refrigeration **21** (1998), 398 – 414.

[8] N.E. Todreas and M.S Kazimi, *Nuclear Systems I, Thermal Hydraulic Fundamentals*, Taylor and Francis, 1993.

[9] P.B. Whalley, *Boiling, Condensation and Gas-Liquid Flow*, 1987.